



Article

Investigating the Response of Vegetation to Flash Droughts by Using Cross-Spectral Analysis and an Evapotranspiration-Based Drought Index

Peng Li ^{1,2,3} , Li Jia ^{1,2,*} , Jing Lu ¹ , Min Jiang ¹ , Chaolei Zheng ¹ and Massimo Menenti ^{1,4}

- ¹ Key Laboratory of Remote Sensing and Digital Earth, Aerospace Information Research Institute, Chinese Academy of Sciences, Beijing 100101, China; lipeng@radi.ac.cn (P.L.); lujing@aircas.ac.cn (J.L.); jiangmin@aircas.ac.cn (M.J.); zhengcl@aircas.ac.cn (C.Z.); m.menenti@radi.ac.cn (M.M.)
- ² International Research Center of Big Data for Sustainable Development Goals, Beijing 100094, China
- ³ University of Chinese Academy of Sciences, Beijing 100049, China
- ⁴ Faculty of Civil Engineering and Geosciences, Delft University of Technology, Stevinweg 1, 2825 CN Delft, The Netherlands
- * Correspondence: jiali@aircas.ac.cn

Abstract: Flash droughts tend to cause severe damage to agriculture due to their characteristics of sudden onset and rapid intensification. Early detection of the response of vegetation to flash droughts is of utmost importance in mitigating the effects of flash droughts, as it can provide a scientific basis for establishing an early warning system. The commonly used method of determining the response time of vegetation to flash drought, based on the response time index or the correlation between the precipitation anomaly and vegetation growth anomaly, leads to the late detection of irreversible drought effects on vegetation, which may not be sufficient for use in analyzing the response of vegetation to flash drought for early warning. The evapotranspiration-based (ET-based) drought indices are an effective indicator for identifying and monitoring flash drought. This study proposes a novel approach that applies cross-spectral analysis to an ET-based drought index, i.e., Evaporative Stress Anomaly Index (ESAI), as the forcing and a vegetation-based drought index, i.e., Normalized Vegetation Anomaly Index (NVAI), as the response, both from medium-resolution remote sensing data, to estimate the time lag of the response of vegetation vitality status to flash drought. An experiment on the novel method was carried out in North China during March–September for the period of 2001–2020 using remote sensing products at 1 km spatial resolution. The results show that the average time lag of the response of vegetation to water availability during flash droughts estimated by the cross-spectral analysis over North China in 2001–2020 was 5.9 days, which is shorter than the results measured by the widely used response time index (26.5 days). The main difference between the phase lag from the cross-spectral analysis method and the response time from the response time index method lies in the fundamental processes behind the definitions of the vegetation response in the two methods, i.e., a subtle and dynamic fluctuation signature in the response signal (vegetation-based drought index) that correlates with the fluctuation in the forcing signal (ET-based drought index) versus an irreversible impact indicated by a negative NDVI anomaly. The time lag of the response of vegetation to flash droughts varied with vegetation types and irrigation conditions. The average time lag for rainfed cropland, irrigated cropland, grassland, and forest in North China was 5.4, 5.8, 6.1, and 6.9 days, respectively. Forests have a longer response time to flash droughts than grasses and crops due to their deeper root systems, and irrigation can mitigate the impacts of flash droughts. Our method, based on cross-spectral analysis and the ET-based drought index, is innovative and can provide an earlier warning of impending drought impacts, rather than waiting for the irreversible impacts to occur. The information detected at an earlier stage of flash droughts can help decision makers in developing more effective and timely strategies to mitigate the impact of flash droughts on ecosystems.

Keywords: flash drought; cross-spectral analysis; ET-based drought index; vegetation response; time lag



Citation: Li, P.; Jia, L.; Lu, J.; Jiang, M.; Zheng, C.; Menenti, M. Investigating the Response of Vegetation to Flash Droughts by Using Cross-Spectral Analysis and an Evapotranspiration-Based Drought Index. *Remote Sens.* **2024**, *16*, 1564. <https://doi.org/10.3390/rs16091564>

Academic Editor: Gabriel Senay

Received: 7 March 2024

Revised: 13 April 2024

Accepted: 17 April 2024

Published: 28 April 2024



Copyright: © 2024 by the authors. Licensee MDPI, Basel, Switzerland. This article is an open access article distributed under the terms and conditions of the Creative Commons Attribution (CC BY) license (<https://creativecommons.org/licenses/by/4.0/>).

1. Introduction

Traditionally, drought is often seen as a slowly evolving natural phenomenon caused by a lack of precipitation over some period [1]. Recently, flash drought, characterized by a sudden onset and rapid intensification with destructive impact, has drawn significant attention [2–6]. In addition to precipitation deficits, flash droughts are often accompanied by abnormally high air temperature, low humidity, strong solar radiation, and sometimes strong winds that intensify the rapid depletion of soil moisture [7–9]. The rapid onset of flash droughts leaves insufficient time to deal with their impacts, which can be more destructive to vegetation, especially agricultural crops, than a more slowly developing drought [10]. In recent decades, with global warming, flash droughts are becoming more frequent, and their impacts are becoming more severe [11–14]. For example, the flash drought that occurred in 2010 in southwestern Russia resulted in a grain harvest dropping to less than half the previous year [15]. The 2017 flash drought in the northern Great Plains of the US destroyed major field crops, leading to significant yield losses in corn and soybeans [16]. The flash drought that occurred in the Yangtze River basin in China during August–October 2022 destroyed crop growth and caused billions of dollars in economic losses [17]. Although the damage caused by flash droughts has increased over the last decade, there is still a lack of understanding of how vegetation responds to flash droughts. Quantifying the response of vegetation to flash droughts is crucial for the development and implementation of drought early warning systems.

In past decades, several remote sensing-based methods for monitoring droughts have been developed, including methods based on vegetation indices, canopy temperature, evapotranspiration, and microwave signals, and widely applied worldwide [18–27]. The vegetation indices (VIs), such as the Normalized Difference Vegetation Index (NDVI) and the Enhanced Vegetation Index (EVI), have been widely used to develop drought indices or indicators to monitor vegetation health and assess the effect of water stress on vegetation [20–22]. Drought indicators based on vegetation index measure the stress and the damage to vegetation vitality caused by drought after a period of drought development [28]. In most previous studies, the time-lagged correlation analysis was widely used to explore the response time of vegetation to drought by identifying the lagged time with the maximum correlation coefficient between the NDVI anomaly and precipitation anomaly or precipitation-based drought indices [29–33]. However, correlation analysis does not provide accurate estimates of time lags, due to the complex non-linear relationship between the vegetation activity and the environmental factors that caused droughts [34–36].

The response time index can determine the timing of the initial occurrence of the negative anomaly in the vegetation growth condition affected by flash drought, which has been widely used to explore the impact of flash drought on the ecosystem [37–42]. Zhang and Yuan [37] assessed the response of ecosystems to flash drought using the response time index based on observations at FLUXNET stations, demonstrating that there is a significant difference in response time between savanna and forest. Zhang et al. [38] examined the response of ecosystems to flash droughts in China using the response time index based on MODIS satellite observations, showing that the net primary productivity (NPP) is more sensitive to the occurrence of flash drought than the gross primary productivity (GPP) and leaf area index (LAI), which is attributed to the vegetation respiratory process and physiological process of photosynthesis.

Previous studies show that the response time of vegetation to drought, as measured by methods based on time-lagged correlation analysis or the response time index, ranges from a dozen days to a few months [29,31,32,37–39,43–45]. Although these methods are easy to apply, they provide a response time when the ecosystem has experienced the destruction of plant vitality. Such information on response time may not be useful in planning and deploying appropriate interventions for drought, due to the irreversibility of the impact. It is essential to understand the dynamic response of vegetation to water availability during the course of a flash drought so that vegetation stress can be detected in time for appropriate intervention before the ecosystem reaches irreversible damage; this is particularly crucial

for mitigating the impact of flash droughts on agricultural yields. Previous studies have proved that spectral analysis can quantify the time lag of the response of vegetation to droughts [46–48]. van Hoek et al. [47] successfully applied cross-spectral analysis to long-term satellite precipitation and NDVI data in northeastern China to investigate the temporal response of the vegetation growth anomaly determined by the Normalized Vegetation Anomaly Index (NVAI) to the precipitation anomaly. Therefore, an alternative method is to use cross-spectral analysis, which simultaneously provides the strength of the relationship and the phase lag for all significant periodic components of the forcing and response signals, and is thus an effective method for quantifying the dynamic response of vegetation ecosystems to flash droughts.

Several studies have investigated the relationship between satellite-derived vegetation indices and flash drought identified by the rapid change in root-zone soil moisture [37–39,42]. The root-zone soil moisture data, however, have typically been derived from coarse spatial datasets (e.g., 0.125° to 0.5°) based on land surface models, which limits the ability to provide fine-scale spatial patterns of flash droughts at the ecosystem scale. Drought indices based on the ET fraction—the ratio of actual evapotranspiration (AET) to potential evapotranspiration (PET) and related to available soil water, atmospheric water demand, and available energy—are sensitive to rapidly changing soil moisture and have been considered an appropriate alternative to drought indicators based on root-zone soil moisture for monitoring flash droughts [8,27,49–51]. ET-based drought indices, such as ESI (Evaporative Stress Index), are metrics of anomalies in the ET fraction and can effectively characterize soil moisture availability [27,52]. In addition, studies suggest that ET-based drought indices, such as ESI and ESP [27,53], may provide better early warnings of drought than NDVI anomalies, which may be used as metrics of water availability during droughts [8,28,53].

In recent decades, many regional and global-scale evapotranspiration data products with the advantage of much higher spatial resolution (e.g., up to 1 km or even higher) have been developed based on satellite observations and are more easily accessible, such as the MODIS ET products [54] and the ETMonitor product [55,56]. Such data can be easily applied to any ET-based drought indicator and will certainly benefit the identification of the response of vegetation to flash drought at higher spatial resolution compared to that based on root-zone soil moisture datasets with coarse spatial resolution. The ETMonitor model has been developed based on a multi-process parameterization scheme to estimate the evapotranspiration components of evapotranspiration (i.e., vegetation transpiration, canopy rainfall interception loss, soil evaporation, water surface evaporation, snow and ice sublimation), taking into account the simulation of the energy balance, water balance, and plant physiological processes that control the water flux exchange at the land surface–atmosphere interface [55,56]. The ETMonitor product provides a spatiotemporal continuous distribution of actual evapotranspiration at moderate spatial resolution (i.e., 1 km), which can describe the consistent spatiotemporal variability in actual ET. Studies have shown that the ETMonitor products have good agreement with in situ measurements from global flux tower sites, and perform better particularly in presenting the spatial variation in ET in irrigated croplands and mountainous regions with complex terrain [57,58]. Comparison studies over Africa and Thailand also showed the good quality of the ETMonitor product [57,58].

Therefore, in this study, we proposed a novel algorithm that applies the cross-spectral analysis to the ET-based index as an indicator of water availability (forcing signal) and the vegetation anomaly index as an indicator of the response signal, both based on remote sensing observations at moderate spatial resolution (i.e., 1 km), to investigate the dynamic response of vegetation vigor to water availability during flash droughts. Specifically, this research includes (1) applying the ESP-based method to identify flash drought in North China over 2001–2020; (2) proposing a novel method that applies cross-spectral analysis to an ET-based drought index and vegetation-based drought index from remote sensing data to quantify the response time lag of vegetation to flash droughts; (3) assessing the response time lag from the cross-spectral analysis and the response time from the

previously established response time index method for further understanding the response of vegetation to flash droughts; and (4) investigating the difference in the response of different vegetation types to flash droughts.

The innovation of our study is twofold: (a) the use of ET-based indicators to identify flash drought events and to characterize water availability during drought events, and (b) the use of cross-spectral analysis to quantify the dynamic response of vegetation vigor condition to water availability during drought events. Our method provides a finer insight into the variability in the response of vegetation to water availability during a flash drought, i.e., how much time do fluctuations in vegetation vigor conditions (i.e., NDVI anomaly) lag behind fluctuations in water availability (i.e., ET-based drought index), which can capture the response of vegetation to water stress much earlier than using the widely used method (i.e., response time index).

2. Study Area and Materials

2.1. Study Area

The North China area was selected for this study because it is prone to drought. It includes Hebei province, northern Henan province, Shandong province, Shanxi province, Beijing, and Tianjin (Figure 1a,b). It belongs to the semi-humid and semi-arid continental monsoon climate zone, with an annual mean temperature of 10.0–14.2 °C and an annual mean precipitation of 500–1000 mm (Figure 1b). About 70% of the precipitation in the study area occurs during the summer months (June–September) due to the monsoon climate. The elevation provided by SRTM 90 m digital elevation data in the study area ranges from 0 to 2882 m (Figure 1c). The western part of the study area mainly included the Shanxi province and western part of Hebei province, with significantly higher altitudes than the eastern part. Future climate change is expected to amplify the risk, severity, and frequency of droughts in North China, thereby exacerbating the impacts on local ecosystems and crop production [59]. Consequently, there is an urgent need to investigate the characteristics of flash droughts over North China.

North China is the major grain-producing area in China, mainly producing maize, wheat, cotton, soybean, etc. This region produces 61% of wheat, 45% of corn, and 35% of cotton in China. From an agricultural perspective, drought occurs when soil moisture is insufficient in meeting the crop water requirements, resulting in yield losses. Crop water requirements vary according to weather conditions and crop growth stages. The prevailing irrigation schedule is designed to meet the water requirements of the double cropping system with winter wheat and summer maize. The growing season for winter wheat is typically from November to May, while the growing period for summer maize is from June to August. In rainfed agriculture, it is common to cultivate only one crop per year, such as spring maize or cotton. The growing period for spring maize is typically from April to August.

2.2. ET Dataset

To identify and monitor flash drought, we used ET derived from the ETMonitor dataset based on multi-source remote sensing (https://data.casearth.cn/thematic/GWRD_2023/272 (accessed on 1 April 2023)). The ETMonitor model estimates actual ET by integrating plant transpiration, soil evaporation, vegetation canopy interception loss, water body evaporation, and snow/ice sublimation, by considering the simulation of the energy balance, water balance, and plant physiological processes that control the surface energy and water exchanges [55]. ETMonitor is suitable for ET estimation under both homogeneous and heterogeneous land surfaces [55,60], and it has been successfully applied at medium–high resolution for various applications [61,62]. The validation result based on flux observations from 251 ground flux sites around the world showed that the Root-Mean-Square Error of daily ET from the ETMonitor product was 0.93 mm/day, which is better than other mainstream global ET datasets [55]. Meanwhile, ETMonitor ET can capture the seasonal dynamics of ET in water and snow-covered regions and performs better in presenting the

spatial variation in ET in the irrigated cropland regions and mountainous regions with complex terrain. The potential ET (PET) is also estimated using the Food and Agriculture Organization Penman–Monteith equation [63]. Both the actual ET and PET from 2000 to 2021 have a spatial resolution of 1 km and temporal resolution of daily.

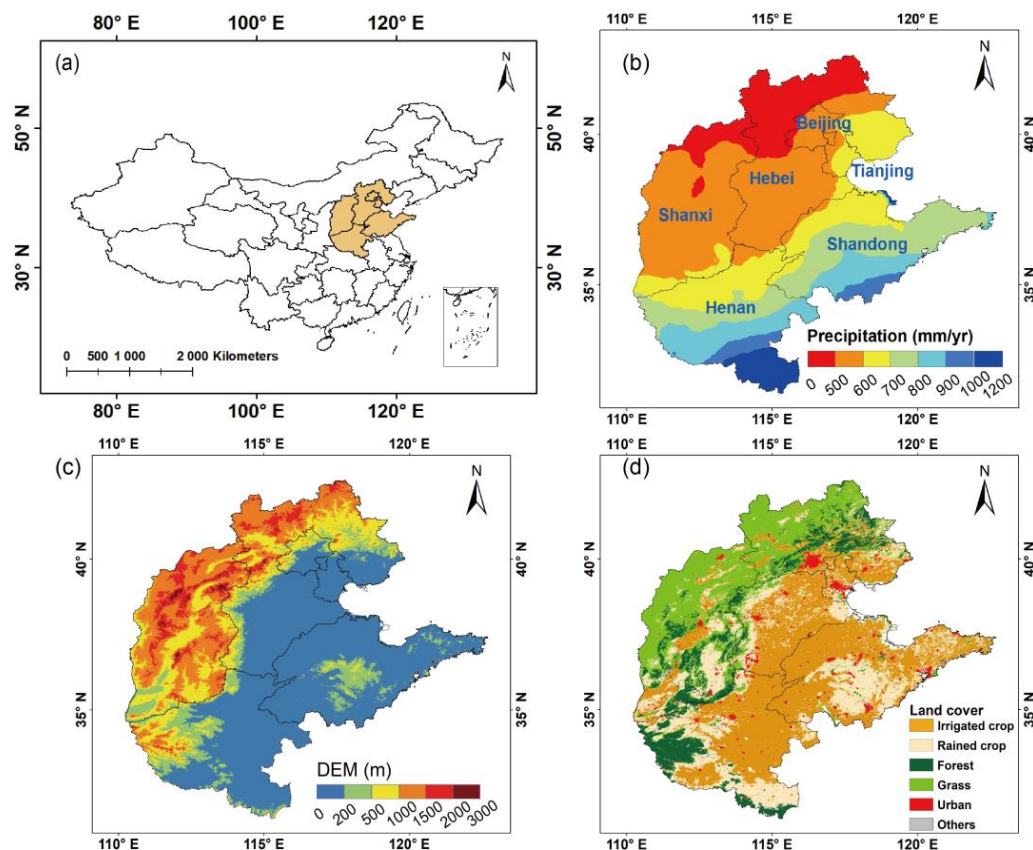


Figure 1. The spatial distribution of (a) location in China; (b) mean annual precipitation (mm/year); (c) altitudes (m); (d) land cover in 2019 from MCD12Q1 and IrriMap CN dataset over North China. The mean annual precipitation was calculated using the Global Precipitation Measurement (GPM) precipitation data product for the period 2001–2020.

2.3. Land Cover and Irrigation Datasets

To explore the response of different vegetation types to flash droughts, we used the MODIS land cover products (MCD12Q1) based on the international geosphere biosphere program (IGBP) classification (<https://search.earthdata.nasa.gov/> (accessed on 1 January 2023)). The MCD12Q1 V6 product provides global land cover types annually with a spatial resolution of 500 m derived from six different classification schemes for 2001–present. To facilitate the follow-up analysis, the 17 categories of IGBP were aggregated into six categories, as shown in Table 1. The LULC data were resampled to 1 km resolution.

The MCD12Q1 land use dataset does not explicitly differentiate between irrigated and rainfed croplands. In this study, we used the irrigated cropland maps in 2019 across China derived from IrriMap_CN (<http://doi.org/10.6084/m9.figshare.20363115> (accessed on 1 June 2023)). The IrriMap_CN dataset provides annual irrigated cropland maps with a 500 m resolution across China for 2000–2019 [64,65]. To match the spatial scale, this irrigated cropland map in 2019 was resampled to 1 km resolution by using the majority resampling method, which calculated the fractions of land cover classes in each 1 km pixel using the 500 m resolution data and assigned the land cover class according to the largest fraction of the land cover class for each 1 km grid. Generally, the vegetation in this study area mainly consists of forest, rainfed cropland, irrigated cropland, grassland, and others which occupy

5%, 21%, 44%, 14%, and 16% of the total study area, respectively. The land cover used in this study is shown in Figure 1d.

Table 1. The original IGBP classification and reclassification of land use.

Class	IGBP Classes	Reclassification
1	Evergreen needleleaf forests	Forest
2	Evergreen broadleaf forests	Forest
3	Deciduous needleleaf forests	Forest
4	Deciduous broadleaf forests	Forest
5	Mixed forests	Forest
6	Closed shrublands	Others
7	Opened shrublands	Others
8	Woody savannas	Forest
9	Savannas	Forest
10	Grasslands	Grassland
11	Permanent wetlands	water
12	Croplands	Cropland
13	Urban and built-up	Urban
14	Cropland/natural vegetation mosaic	Cropland
15	Snow and ice	Others
16	Barren and sparsely vegetated	Others
17	Water bodies	water

2.4. NDVI Dataset

The Moderate Resolution Imaging Spectroradiometer (MODIS) vegetation indices product (MOD13A2 V6.1) (<https://search.earthdata.nasa.gov/> (accessed on 1 January 2023)) provides the Normalized Difference Vegetation Index (NDVI) at a 1 km resolution every 16 days. We applied the iHANTS (improved Harmonic Analysis of Time Series) method [66] to reconstruct daily values of NDVI from the original 16-day NDVI data (MOD13A2 V6.1). The time series of daily NDVI at 1 km for the period of 1 January 2001–31 December 2020 were generated. The iHANTS (improved Harmonic Analysis of Time Series) method was updated from the original HANTS based on the Fourier transform, which is commonly used in remote sensing image processing to reconstruct the missing data and remove the noise [66–72]. The reconstructed daily NDVI did correctly capture the phenology response of each land cover type, as shown in Figure 2. Irrigated cropland has two crop cycles in a year, whereas rainfed cropland has only one crop cycle per year.

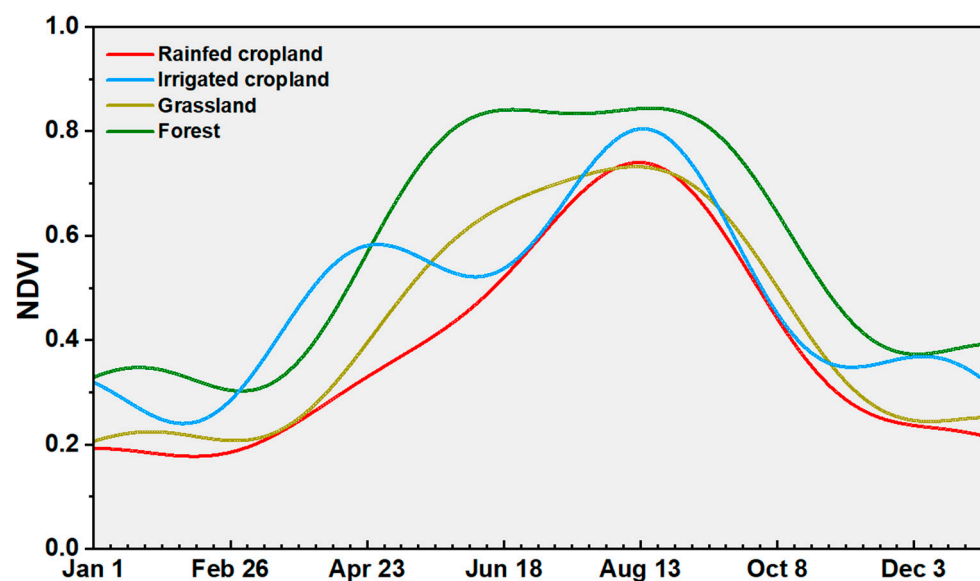


Figure 2. NDVI time series curves of different vegetation types over North China.

3. Methods

This paper proposes a new method to quantify the response of vegetation conditions to water availability during flash droughts by applying cross-spectral analysis to the vegetation-index-based drought indicator (i.e., the Normalized Vegetation Anomaly Index, NVAI) and an ET-based flash drought index (i.e., evaporative stress percentile, ESP). The ESP describes the water availability. This method was applied over North China in the growing season (March–September) during the period of 2001–2020. The workflow is presented in Figure 3, and it consists following steps:

- (1) Drought index calculation, which estimates the Evaporative Stress Anomaly Index (ESAI) based on ET from the ETMonitor dataset and the Normalized Vegetation Anomaly Index (NVAI) based on the reconstructed daily NDVI dataset.
- (2) Flash drought identification, which identifies flash drought events and their characteristics using the Evaporative Stress Percentile (ESP) using ET from the ETMonitor dataset.
- (3) Detection of the vegetation response to water availability during flash drought, which applies the cross-spectral analysis method to detect the time lag between NVAI and ESAI.
- (4) Analysis of the advantages of the proposed method, which is compared with the results using the response time index method.

We applied the 7-day moving window average to reduce the noise in the time series of ET and the NDVI and to ensure the cross-spectral method can extract the information on the response of the vegetation anomaly to the water availability.

Detailed information on each step is presented in the following sections.

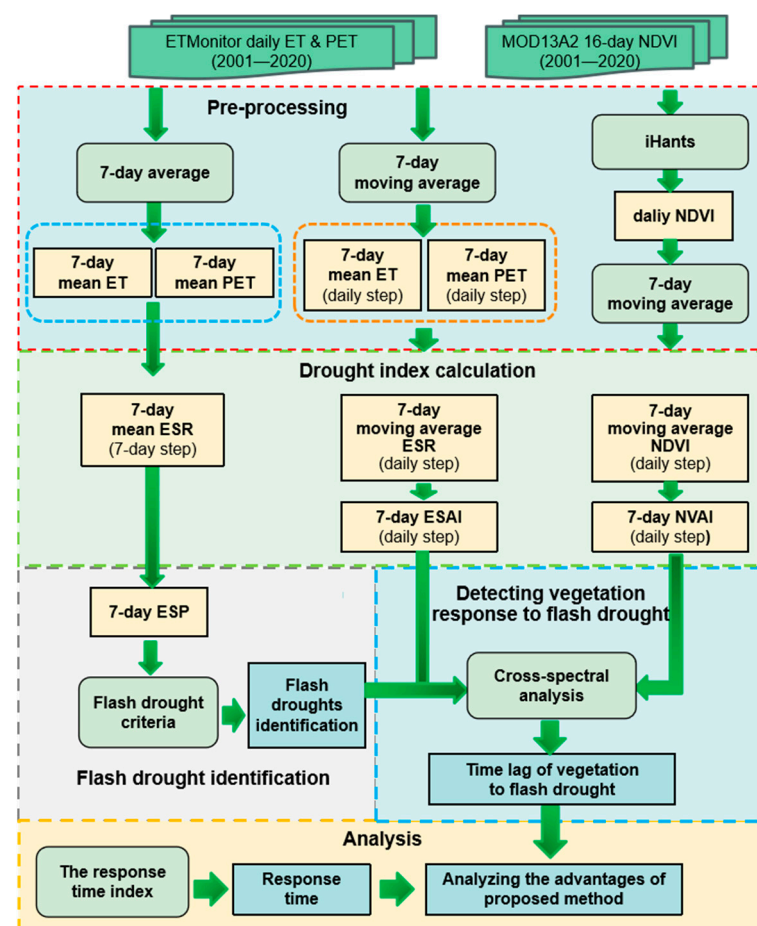


Figure 3. Workflow of this study.

3.1. Drought Index Calculation

3.1.1. Evaporative Stress Anomaly Index

The evaporative stress ratio (*ESR*) is expressed as the physical relationship between the actual evapotranspiration and potential evapotranspiration as follows [73]:

$$ESR = \frac{AET}{PET} \quad (1)$$

where *AET* is the actual evapotranspiration and *PET* is the potential evaporation. The *ESR* ranges from zero to one, indicating the water availability of an ecosystem from insufficient water supply to optimal water conditions. In this study, the daily ET and *PET* time series from the ETMonitor dataset during 2001–2020 were used and smoothed by applying a 7-day moving average filter to obtain a 7-day moving average *ESR* in daily steps. The 7-day average *ESR* in daily steps was obtained using the ratio of 7-day ET to 7-day *PET*.

The Evaporative Stress Anomaly Index (*ESAI*) presents standardized anomalies of *ESR* and can effectively capture flash drought events. The *ESAI* is defined as

$$ESAI = \frac{ESR - ESR_{mean}}{ESR_{max} - ESR_{min}} \quad (2)$$

where *ESR*, *ESR_{mean}*, *ESR_{max}*, and *ESR_{min}* are the current, multi-year average, historical maximum, and historical minimum values of *ESR*, respectively, for a given time period (e.g., daily, weekly, or monthly) and for each pixel. The *ESAI* varies from −1 to 1. Negative *ESAI* values indicate that vegetation is experiencing water stress, while positive *ESAI* values indicate favorable moisture conditions or sufficient water availability. In this study, the daily ET and *PET* time series from the ETMonitor dataset during 2001–2020 were first smoothed by applying a 7-day moving window filter to obtain a 7-day moving average *ESR* with a daily time step. By using a daily time step, the *ESAI* drought index retains the higher temporal resolution. The 7-day moving average *ESR* in daily steps was then applied to Equation (2) to obtain the daily step *ESAI* to be used in cross-spectral analysis.

3.1.2. Normalized Vegetation Anomaly Index

The vegetation health condition responds to drought and can be captured by vegetation-index-based drought indicators. The *NVAI* evaluates the current *NDVI* in comparison to the values in the same period in history, as defined by [20]

$$NVAI = \frac{NDVI - NDVI_{mean}}{NDVI_{max} - NDVI_{min}} \quad (3)$$

where *NDVI*, *NDVI_{mean}*, *NDVI_{max}*, and *NDVI_{min}* are the current, historical average, historical maximum, and historical minimum *NDVI*, respectively, for a given period and pixel. The *NVAI* ranges from −1 to 1, characterizing changes in vegetation conditions from extremely poor (−1) to favorable (1). In this study, we applied iHANTS [66] to the original 16-day *NDVI* data (MOD13A2 V6.1) to obtain daily *NDVI*, and then applied a 7-day moving average filter to obtain the 7-day moving average *NDVI* in daily steps. The 7-day moving average *NDVI* in daily steps was then applied to Equation (3) to obtain the daily step *NVAI* to be used in cross-spectral analysis.

3.2. Identification and Characteristics of Flash Drought

3.2.1. Flash Drought Identification

The Evaporative Stress Percentile (*ESP*) is the percentile of *ESR* of a period (e.g., weekly) over the historical record of *ESR* in the same period in each pixel, which is proposed by Li et al. [53] to detect flash drought. The *ESP* was calculated using the cumulative distribution function of *ESR* (Figure 4). The *ESP* value that falls below a given value can be linked to the severity of drought; the lower the *ESP*, the drier the condition compared to

the historical record. Three criteria based on the weekly ESP are established to identify a flash drought event [53]:

- (1) Onset: the ESP decreases from above the 40th percentile to below the 20th percentile with an average decline rate of no less than 6.5 percentile/week.
- (2) Termination: the flash drought terminates when the ESP value rises above the 20th percentile and lasts for at least two weeks.
- (3) Duration: flash droughts should last for at least 3 weeks.

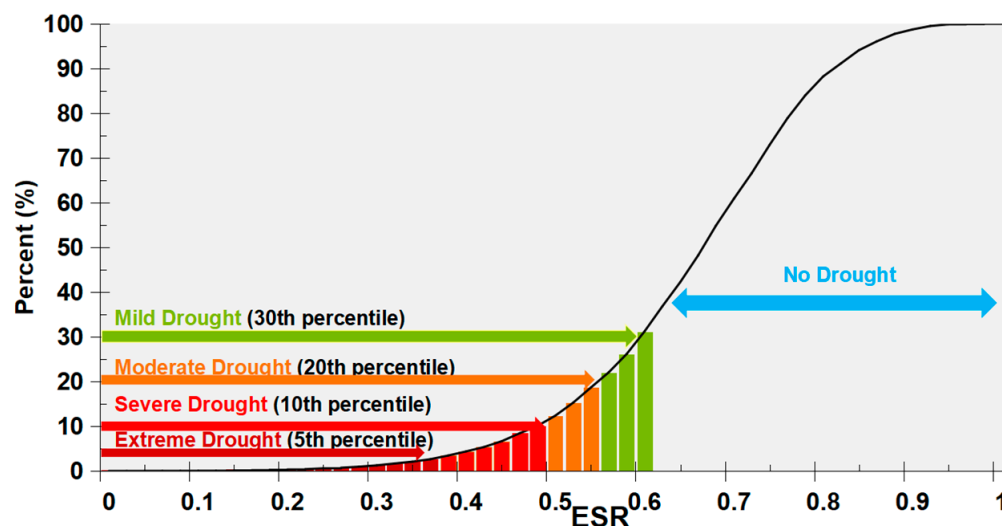


Figure 4. Illustration of the ESP values corresponding to drought severity.

In this study, the ESP was calculated using the ETMonitor ET dataset and applied to identify flash droughts over North China in the growing season (March–September) during the period of 2001–2020.

3.2.2. Characteristics of Flash Drought

In this study, we investigated the spatiotemporal characteristics (numbers and average duration) of flash droughts over North China during the growing season (March–September) for the period of 2001–2020 based on the ESP. The characteristics of the flash droughts can be described as follows:

- (1) The number of flash droughts: the total number of flash drought events over the selected study period.
- (2) The duration of the flash drought: the number of days from the onset (the ESP dropped to below the 20th percentile) to the recovery (ESP above the 20th percentile again).

3.3. Cross-Spectral Method

Cross-spectral analysis has been applied to multiple scientific research fields, which can simultaneously study the relationship and corresponding time lag between two stationary time series in the frequency domain [74,75]. This means that the oscillations in a forcing signal precede the oscillations in the response signal. The cross-spectral analysis was applied to the time series of ESAI and NVAI for each flash drought event identified by the ESP-based approach (see Section 3.2) to investigate the response of vegetation to flash drought over North China during the growing season (March–September) from 2001 to 2020. More precisely, the cross-spectral analysis provides a measure of the response of oscillations in NVAI to oscillations in ESAI during each drought event. The specific steps and detailed explanation of cross-spectral analysis are detailed below [47,76]:

(1) Cross-coherence

Cross-coherence is a measure of the correspondence between the spectra of two signals:

$$C_{xy}(f) = \frac{|P_{xy}(f)|^2}{P_{xx}(f)P_{yy}(f)} \quad (4)$$

where $P_{xy}(f)$ is the cross-power spectral density between two signals $x(t)$ and $y(t)$ in the frequency domain. $P_{xx}(f)$ and $P_{yy}(f)$ are the auto-spectral densities of signals $x(t)$ and $y(t)$ at frequency f , respectively. The coherence value varies from 0 to 1. A coherence value of 1 indicates that the signals are highly correlated or related at that frequency. Conversely, a coherence of 0 indicates that the two signals have unrelated spectral components at that frequency.

(2) Gain:

The gain is the measure of the contribution of a specific frequency component from one signal in the cross-spectrum of two signals. It provides information about how the power or amplitude of a particular frequency component in one signal contributes to the overall cross-spectrum of another signal, which is defined as

$$C_{xy}(f) = \frac{|P_{xy}(f)|^2}{\sqrt{P_{xx}(f)}} \quad (5)$$

where $P_{xy}(f)$ is the cross-power spectral density between two signals $x(t)$ and $y(t)$ in the frequency domain. $P_{xx}(f)$ is the auto-spectral density of signal $x(t)$ at frequency f . A higher amplitude in the gain indicates that the first signal contributes more to the cross-spectrum at that particular frequency.

(3) Phase spectrum

The phase spectrum is expressed in radians, which represents the phase difference between signals x and y at a given frequency. The time lag ($\Phi_{xy}(t)$) is expressed in units of days and obtained from the phase spectrum as

$$\Phi_{xy}(t) = \frac{\tan^{-1} \frac{\text{img}(P_{xy}(f))}{\text{real}(P_{xy}(f))}}{2\pi f} \quad (6)$$

where $\text{img}(P_{xy})$ is the imaginary part of $P_{xy}(f)$ and $\text{real}(P_{xy}(f))$ is the real part of $P_{xy}(f)$.

(4) Consistency test

To estimate the uncertainty of the phase spectrum, a Monte Carlo simulation was applied by using semi-random sampling to obtain the distribution of the phase spectrum [47]. The semi-random time series of $x(t)_{ran}$, and $y(t)_{ran}$ are created using the following formula:

$$x(t)_{ran} = Z_x(f)e^{+ft} \quad (7)$$

$$y(t)_{ran} = \left(Z_y(f)\sqrt{1-C_{xy}(f)^2} \right) e^{+ft} + Z_x(f)e^{+ft} \quad (8)$$

where $Z_x(f)$ and $Z_y(f)$ are the Fourier transforms of the random realizations of the time series $x(t)$ and $y(t)$ divided by the absolute sum of the norm of each realization, and e^{+ft} represents the inverse Fourier transform. When the two signals do not have a strong correlation at a given frequency, or the sample is insufficient, it will fail to pass the consistency test.

To illustrate the cross-spectral analysis method, two artificial signals were created with a certain visible correlation between the two series (Figure 5). The two time series are presented in Figure 5a. According to the coherence spectrum (Figure 5b), significant

relationships (coherence = 1.0) are identified at 0.05 Hz and 0.1 Hz, corresponding to components with a period of 20 and 10 days, respectively. The 20-day and 10-day components of X lag the components of Y by 2.1 and 8.3 days, respectively (Figure 5d). The gain can more accurately capture the impact of signal components at different frequencies on the relationship between the forcing and response signals, thereby leading to a better understanding of the lag relationship between the signals. According to the gain of the frequency components (Figure 5c), it is found that the 10-day component contributes most to the cross-spectrum of the two signals, accounting for about 92% of the total signal amplitude, while the 20-day component contributes less, accounting for about 8% of the total signal amplitude. The 20-day and 10-day components of X lag the components of Y by 2.1 and 8.3 days, respectively (Figure 5d). The time lag between X and Y is weighted by the gains of the corresponding components. We multiply the time lag corresponding to the 10-day period by 92% and the time lag corresponding to the 20-day period by 8% to obtain the total time lag. This results in X responding to Y with a delay of 7.8 days.

This means that X responds to Y with a delay of 7.8 days. The cross-spectral analysis method was implemented using the Nitime library, an open-source programming language library for Python. This library provides a comprehensive set of tools for time series analysis, including spectral analysis and coherence estimation.

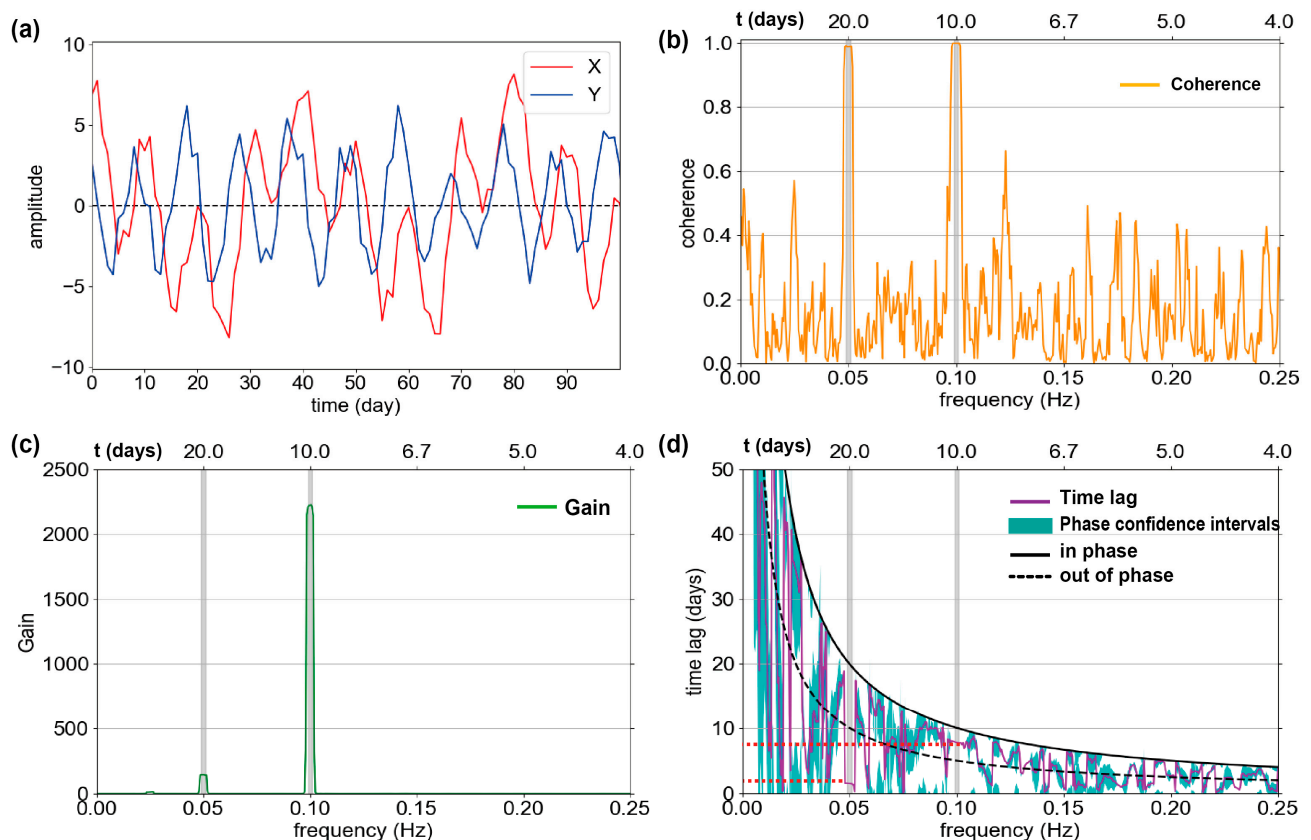


Figure 5. Cross-spectral analysis of time series of two signals with Y as forcing and X as response: (a) Sample time series; (b) the coherence spectrum (with two frequency components with significant relationship marked by the grey vertical lines); (c) gain; (d) the time lag and uncertainty of X and Y signals (the red dashed lines indicate the time lags corresponding to the two frequency components with significant relationship marked by the grey vertical lines).

3.4. Response Time Index

Previous studies used the response time index to qualify the response of vegetation to flash drought [37–42]. In this study, we analyzed the response time derived using response time index method together with the time lag from the spectral analysis method to further

understand the response of vegetation to water availability during the flash droughts. In this study, the ESP-based approach was used to detect the onset of flash droughts and the NVAI was used to assess the impact of flash drought on vegetation health conditions. The vegetation response time to flash drought in the response time index method is defined as the time difference between the onset of flash drought ($t_{20\downarrow}$) and the time at which the NVAI becomes negative (t_N) (Figure 6).

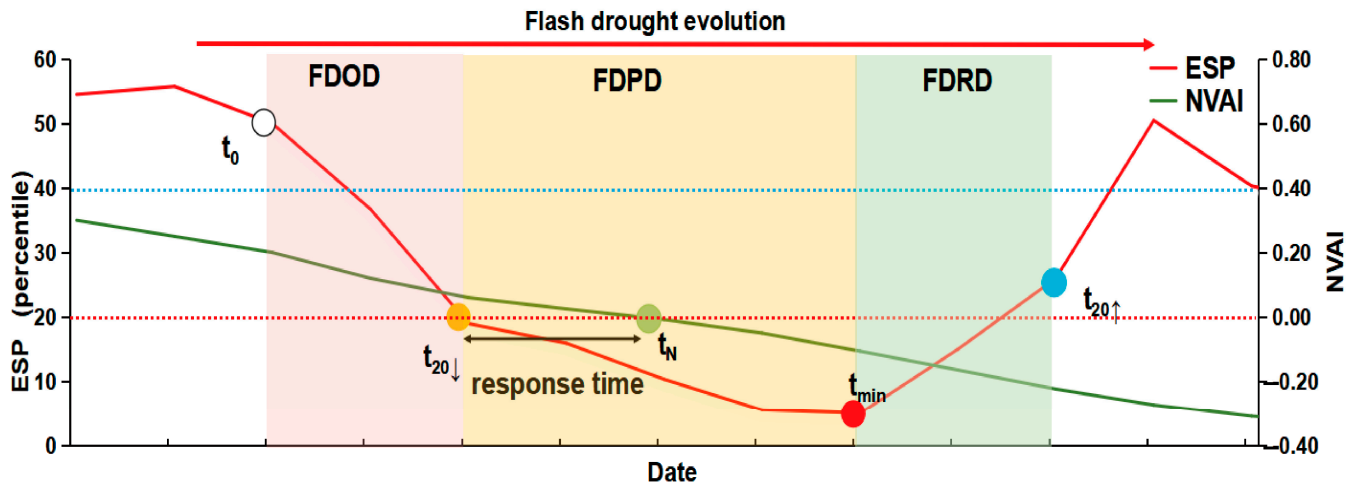


Figure 6. A schematic representation of estimating the response time of vegetation to flash droughts by using ESP and NVAI. During the flash drought onset development duration (FDOD, the light pink area), the soil water condition was drying, and the ESP decreased from above the 40th percentile (at t_0) to below the 20th percentile (at $t_{20\downarrow}$) with an average decline rate of no less than 6.5 percentile/week. The time $t_{20\downarrow}$ is the onset of the flash drought where the ESP falls below the 20th percentile. t_N is the time when NVAI becomes negative for the first time during the flash drought event. The period $t_N - t_{20\downarrow}$ denotes the vegetation response time to flash drought defined by the response time index method. FDPD (flash drought persistence duration; the light orange area) and FDRD (flash drought recovery duration; the light green area) were defined in Li et al. [53]. The blue dashed line indicates the 40th percentile of ESP, and the red dashed line indicates both the 20th percentile of ESP and the zero NVAI.

4. Results

4.1. Flash Droughts over North China from 2001 to 2020

In this section, the Evaporative Stress Percentile (ESP) calculated using the ETMonitor product was applied to analyze the characteristics (frequency and duration) of flash drought over North China in the growing seasons (March–September) during 2001–2020. The specific calculation method for the frequency, duration, and rate of intensification of historical flash droughts is described in Section 3.2.2. During 2001–2020, 14 flash drought events were detected across all of North China (Figure 7a). The areas with fewer than 10 flash drought events in 2001–2020 were mainly located in central Shanxi province, i.e., the eastern part of the Loess Plateau. The hot spot region, which experienced more than 15 drought events in 2001–2020, was in eastern Hebei province, northern and eastern Henan province, and most areas of Shandong province. These areas typically experience dry-hot winds in summer, also known as heat stress, an agrometeorological disaster characterized by high temperature, low humidity, and high wind speed [77], which could increase the likelihood of flash drought developing [78]. The average duration of flash droughts is 37 days over North China, with the longest average durations located over southern Henan province, western Shanxi province, and most areas of Shandong province (Figure 7b). Flash droughts in the southern areas generally last longer than those in the north of North China.

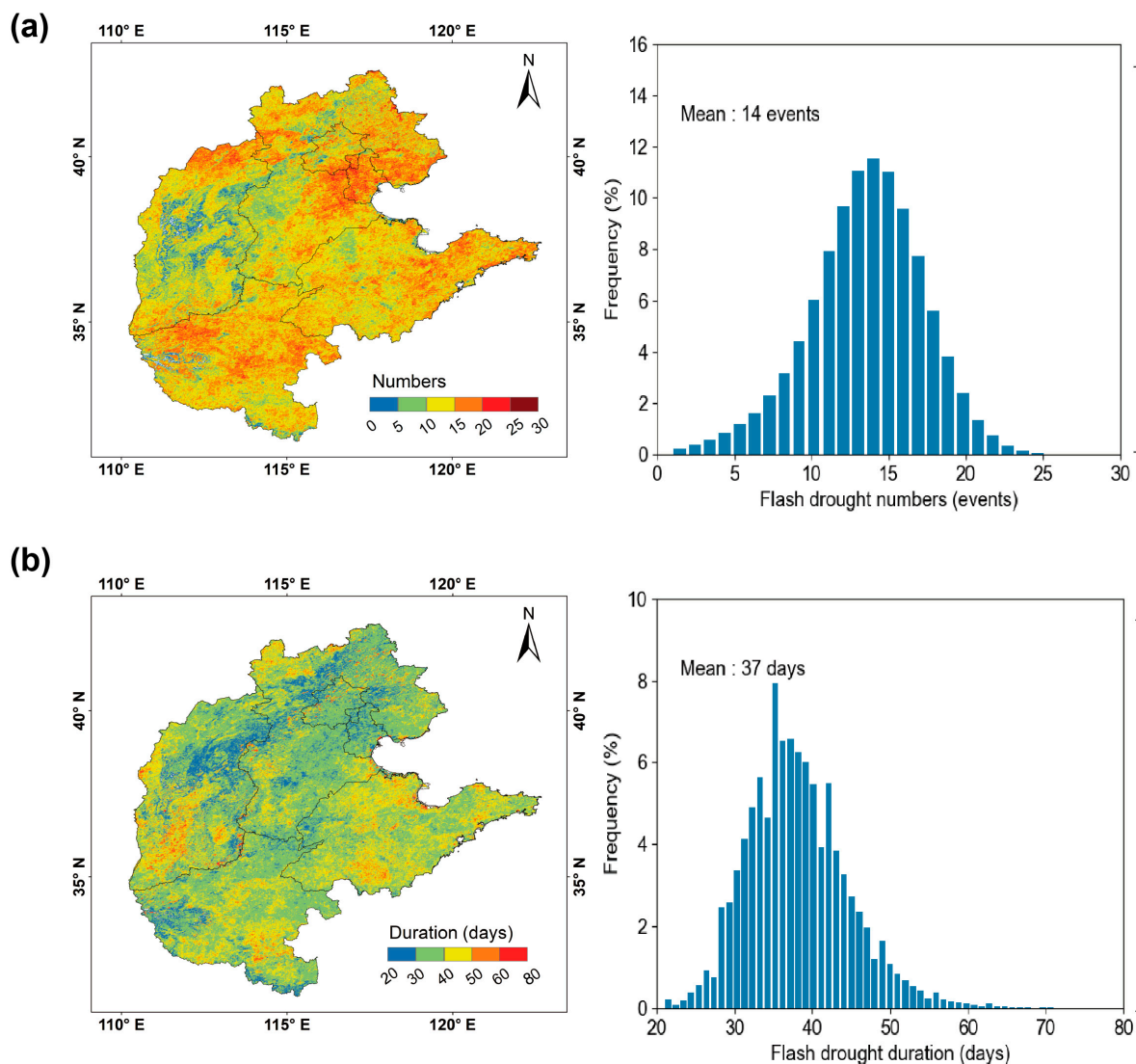


Figure 7. Spatial distribution and the histogram of (a) number and (b) average duration of flash droughts over North China during March–September for the period 2001–2020.

4.2. Time Lag of Vegetation Response to Flash Droughts over North China during March–September for the Period 2001–2020

Having identified flash drought events as documented in Section 4.1, we can now apply two complementary indicators of the response of the vegetation health condition to water availability: the phase (time) lag by the cross-spectral analysis method defined in Section 3.3 and the response time index defined in Section 3.4. The response time index method uses ESP and NVAI to identify the vegetation response time to flash droughts in this study. We focus on flash drought events where vegetation is severely impacted, i.e., NVAI drops below 0 during flash droughts. It should be noted that the response time and the phase (time) lag provide complementary information on the response of vegetation to water availability. The response time indicates how long past the onset of a drought event a clear impact is made on vegetation condition (i.e., a negative NVAI appears). The phase (time) lag provides a finer insight into the variability in vegetation response during a drought event, i.e., how much time are fluctuations in vegetation conditions (i.e., NVAI) lagging behind fluctuations in water availability (i.e., ESAI).

4.2.1. Time Lag Obtained Using Cross-Spectral Analysis

In this section, cross-spectral analysis was applied to NVAI and ESAI time series during flash droughts to investigate in more detail the response of vegetation to fluctuations in water availability (Figure 8a). The time lag in central Henan, northern Hebei, and central Shandong provinces was about 1 to 10 days. In the southern parts of Shanxi, northern Shandong, southern Hebei, and western Henan provinces, the time lag of the response of vegetation to ESAI was about 5 to 20 days. The regional average time lag obtained through cross-spectral analysis was 5.9 days (Figure 8a).

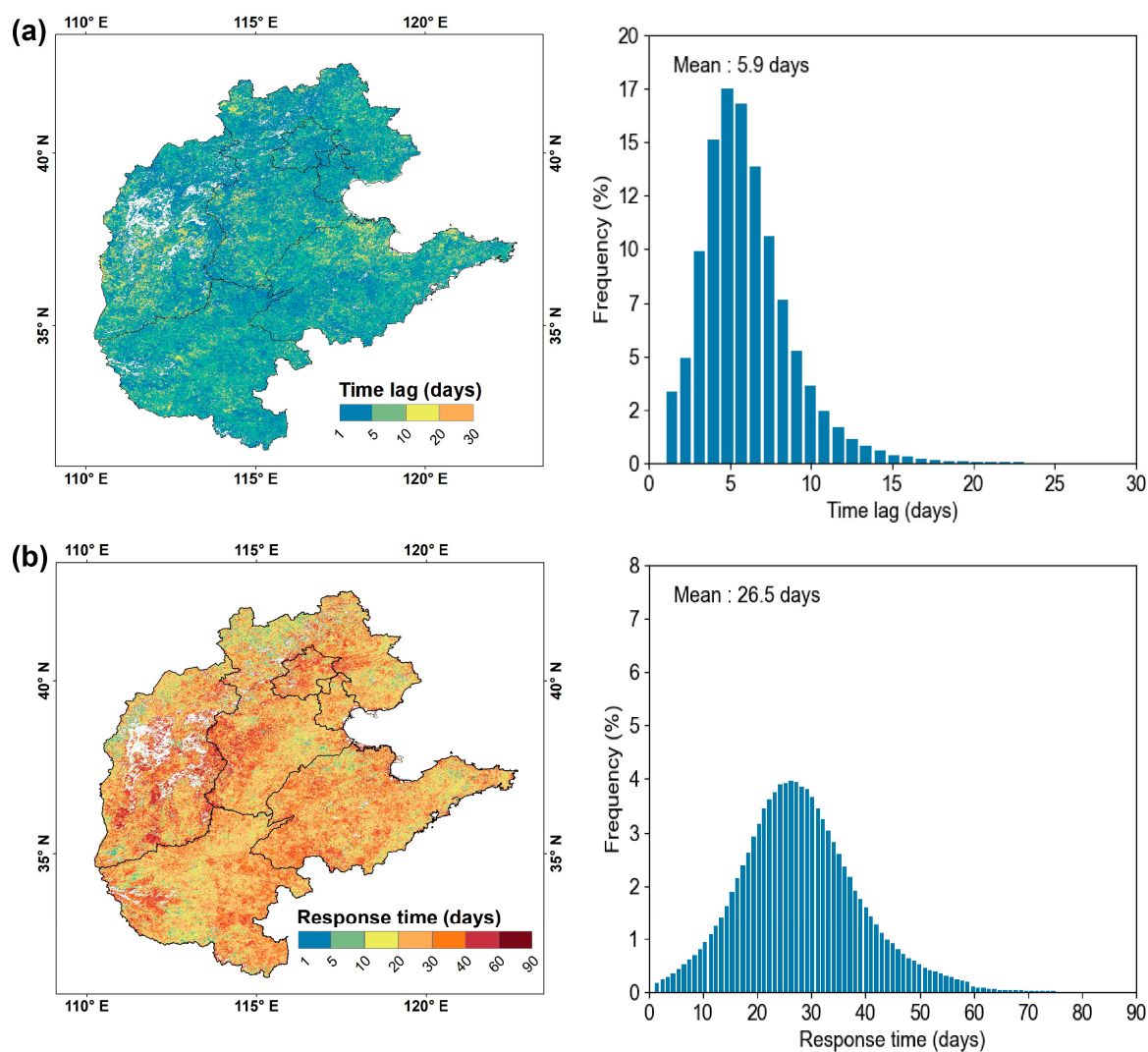


Figure 8. Spatial distribution and histogram of temporal vegetation response to flash droughts over North China during March–September for the period 2001–2020 by using (a) cross-spectral analysis and (b) response time index, respectively (note that blank (white) areas in the spatial maps are areas where the NVAI is above 0, i.e., vegetation was not severely affected during flash droughts).

4.2.2. Combination with the Response Time Index

The response time of vegetation to flash droughts over North China during March–September for the period of 2001–2020 was estimated and its spatial and frequency distributions were evaluated (Figure 8b). The response time in western Henan, northwestern Shandong, western Hebei, and most parts of Shanxi province was more than 20 days. The response time in eastern Shandong province and central Henan province was about 10 to 20 days. The regional average response time was 26.5 days (Figure 8b). Table 2 summarizes the statistics of the time lag from the cross-spectral analysis method and the response time

from the response time index method over the study area for the flash drought events in 2001–2020. It is not surprising that the time lag obtained by using the cross-spectral analysis and the response time index differ greatly: they relate to different processes determining the forcing (ESAI)–response (NVAI) relationship during a given drought event, i.e., an irreversible impact indicated by a negative NVAI vs. a subtle signature in the response signal (NVAI) correlated with the forcing signal (ESAI). The response time is an overall measure of the time difference between the initial stage in the onset of a flash drought event and a likely irreversible impact on vegetation conditions, i.e., a negative NVAI, which highlights vegetation that has been severely affected. The time lag measured by cross-spectral analysis is significantly shorter than the response time, because it is a measure of the resilience of vegetation in adapting to fluctuations in water availability during a drought event. In other words, the time lag reflects the time required for vegetation to respond and adapt to a fluctuation in water availability, i.e., the cross-spectral analysis detects a faster response of vegetation, which might be relevant to prompt drought mitigation actions.

Table 2. The mean time lag from the cross-spectral analysis method and the response time from the response time index method across provinces over the study area for the flash drought events. The values within the parentheses are the range of minimum to maximum values.

	North China	Beijing	Tianjin	Hebei	Shanxi	Shandong	Henan
Time lag (days)	5.9 (1–15.3)	5.8 (1–13.5)	5.2 (1–12.2)	5.7 (1–13.8)	6.1 (1–15.3)	6.2 (1–14.1)	5.9 (1–13.1)
Response time (days)	26.5 (1–61)	28.0 (1–61)	25.5 (2–50)	26.2 (1–56)	28.5 (1–61)	27.0 (2–55)	26.0 (1–55)

4.3. Temporal Response of Different Vegetation Types to Water Availability during Flash Droughts

The temporal response during flash drought events of vegetation types was different (Figure 9). This evaluation was performed by stratifying the maps obtained by using the cross-spectral analysis and response time index for the four main land cover classes over North China. Forest had the longest time lag (mean: 6.8 days), followed by irrigated crop (mean: 6.1 days), rainfed crop (mean: 5.8 days), and grass (mean: 5.4 days) (Figure 9a). With regard to the response time index, forest had the longest response time (mean: 34.7 days), followed by irrigated crop (mean: 27.1 days), rainfed crop (mean: 26.3 days), and grass (mean: 25.9 days) (Figure 9b).

Interestingly, both the time lag and the response time for forests were longer than those for the other vegetation types. Forests typically have deep root systems, allowing them to absorb water from deeper soil layers. As a result, forests can better maintain their water supply during drought periods compared to other vegetation types, thereby delaying the impact of drought on the vegetation, i.e., a longer response time [37,39,79,80]. Likewise, the larger soil water reservoir increases the inertia in the response to fluctuations in water availability, i.e., a longer time lag. In contrast, the time lag for grasslands was shorter than those for other vegetation types. Grasslands, with their shallow root systems, have limited ability to absorb water from deeper soil layers [42,81]. As expected, the response time of irrigated croplands to flash drought was longer than that of rainfed croplands. This can be attributed to the beneficial effects of irrigation in mitigating drought impacts and enhancing the resistance of croplands to drought conditions [82,83]. In most agricultural areas of North China, more than 80% of irrigation water is sourced from groundwater, reducing the reliance of crops on local precipitation [84]. The rainfed cropland is more vulnerable to flash droughts because of limited artificial intervention, and water supply is highly dependent on local precipitation [85].

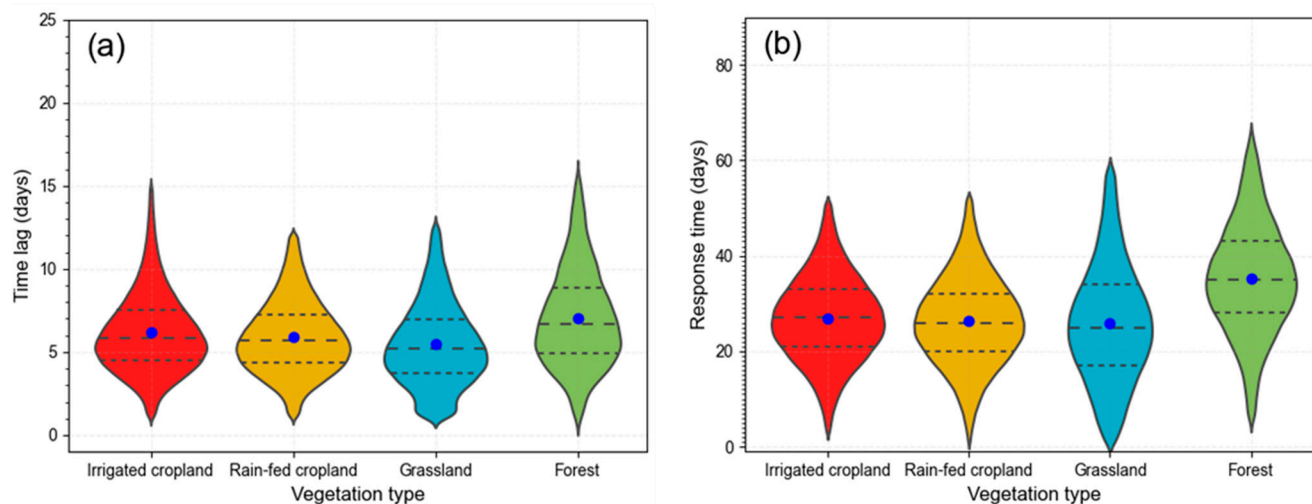


Figure 9. Violin plot of temporal response of vegetation condition (NVAI) of irrigated cropland, rainfed cropland, grassland, and forest to water availability during flash drought events over North China during March–September for the period 2001–2020 by using (a) cross-spectral analysis and (b) response time index. The blue dot shows the mean value, and black dotted lines show the 25th, 50th, and 75th percentile values of each distribution.

5. Discussion

5.1. Advantage of ET-Based Drought Indicator Derived from Satellite Remote Sensing Observations

Flash droughts are often accompanied by precipitation deficits, abnormally high air temperatures, low humidity, and high solar radiation [8,49]. These meteorological factors can quickly increase the atmospheric evaporative demand, thus leading to an increase in transpiration by vegetation, which can rapidly deplete soil moisture. Subsequently, when the soil water supply is insufficient, the AET will rapidly decrease even if these extreme meteorological conditions continue to increase the atmospheric evaporative demand [7]. As soil moisture dry-down continues, flash droughts lead to negative effects on vegetation, such as decreases in photosynthetic activity and canopy vitality [7,80]. Vegetation indices are less able to detect incipient plant stress in the early stages of drought development, because the signal becomes strong after significant damage to the vegetation has already occurred. ET-based drought indices measure anomalies in the ET fraction and can detect incipient plant stress, thus providing an early warning of incipient drought impacts on vegetation. Therefore, vegetation-based drought indicators typically lag behind ET-based drought indicators by several days, even several weeks [8,86]. The time lag is affected by many factors such as vegetation type and soil water retention capacity [47].

Previous studies investigating the response of vegetation to flash droughts have used root-zone soil moisture datasets with coarser grids (e.g., 25–50 km) to identify flash droughts [37–39,42]. In this study, the ET-based drought index based on the ETMonitor product with a finer spatial resolution (1 km) provided a better understanding of the spatial patterns of the response of vegetation to water availability during flash droughts. In addition, previous research on the response of vegetation to drought has rarely focused on the weekly timescale, but rather on the monthly timescale [29,32,44]. The ET-based drought index based on the ETMonitor product provides relatively clean time series showing changes in water availability on a timescale of days.

5.2. Advantage of Cross-Spectral Analysis

Previous studies used the response time index to quantify the temporal response of vegetation to flash drought [31–35]. Although the response time index method is easy to apply, the disadvantage of this method is that it only provides a single, overall measure for each drought event, i.e., the time lag between the onset of a drought and the first negative

anomaly in NDVI, i.e., conditions with a severe impact on vegetation. This seriously limits the development of the early warning system that requires the timeliness monitoring of the response of vegetation to droughts.

This study differs from previous studies in two aspects: the ET-based drought index based on remote sensing data (see discussion in Section 5.1) and cross-spectral analysis. Another unique aspect of this study is the use of cross-spectral analysis. In this study, the time lag during drought events was estimated by cross-spectral analysis of continuous forcing (i.e., ESAI) and response (i.e., NVAI) to explore the finer response of vegetation to fluctuations in water availability during flash drought events. This method has three advantages. Firstly, it provides a better understanding of the response of vegetation to water availability by measuring temporal variability during each drought event. Second, unlike the time response index method and correlation analysis, cross-spectral analysis is applied in the frequency domain and provides independent phase lag estimates for all coherent spectral components of the temporal forcing and response signals through the phase cross-spectrum. Noise appears as small-amplitude components in the frequency domain, which can be filtered out. Last but not least, the time lag estimated through cross-spectral analysis is significantly shorter than that of the response time index. This is due to the inherently different nature of the two temporal metrics. In this study, cross-spectral analysis estimates the time lag between fluctuations in the forcing (i.e., ESAI) and response (i.e., NVAI) signals during each separate drought event. This leads to capturing the fine details in the dynamic response of vegetation conditions to variable water availability during a period of time that is generally drier than normal. Contrariwise, the response time index is an overall estimate of the temporal separation of the onset of a drought event and the appearance of severe impacts, i.e., the first occurrence of a negative NVAI during the drought event. The latter is likely to be associated with an irreversible drought impact on vegetation, limiting the development of an early warning system that requires the timely monitoring of the response of vegetation to droughts. This suggests that our new method using cross-spectral analysis may provide information relevant to the design and deployment of adaptive interventions to mitigate drought impacts by, e.g., sustainable and flexible water resource management.

5.3. Limitations and Future Work

However, our study also has several limitations. It should be noted that the cross-spectral analysis method requires a large number of samples to accurately estimate the spectral density. If the time series are short, the method may produce biased estimates of the spectral density and fail to pass consistency checks. The response of vegetation to flash drought can be influenced by a number of factors, including crop type, soil texture, and irrigation management strategies [87]. In this study, different crops were not treated separately. It should be noted that the cross-spectral analysis implicitly assumes that the underlying processes of the two signals are stationary [88]. This may affect the accuracy of the analysis results if the actual signals do not meet this assumption.

It is challenging to apply the percentile-based approach to datasets with short record periods, as there are insufficient data to represent the statistical distribution [89]. In this study, we used the ESP to identify flash droughts over North China based on a 20-year (2001–2020) span of the remote sensing dataset, and the results showed that the duration of flash droughts ranged from 20 to 50 days, which is comparable to the study from Zhang et al. [12] who investigated the flash droughts in China based on soil moisture over a 40-year period (1981–2021), and found that the duration of flash droughts in the North China Plain ranged from 30 to 50 days. Some studies have also used data from the time span of 20 years and the percentile-based method to identify flash drought [4,78]. Further studies can investigate the uncertainties in identifying flash droughts based on different historical data periods.

With regard to the NDVI limitations, instead of using NDVI values, we used the NDVI anomaly, i.e., the Normalized Vegetation Anomaly Index (NVAI), to represent the vegetation vigor condition, which eliminates the saturation problem of MODIS NDVI over

dense vegetation. Indeed, our research aims to investigate the response of vegetation vigor conditions to flash droughts, and the NDVI-based index is widely used and considered an appropriate parameter to present vegetation vitality. Future work may also evaluate other vegetation indicators, for example, based on GPP and biomass.

There are promising directions for future work to further explore insights into the response of vegetation to flash drought. Given the complex relationship between vegetation conditions and flash drought, future research should focus on machine learning algorithms such as eXtreme Gradient Boosting (XGBoost) [90,91], Random Forest [92,93], SVM [94], and the Convolutional Neural Network (CNN) [95] that can effectively capture their relationships. Among these machine learning methods, the CNN algorithm performs better in feature extraction, pattern recognition, and multi-scale analysis, facilitating the exploration of the relationship between flash drought and vegetation [95]. Future research should also further explore the relationship between vegetation and flash droughts from historical inventory data and ground station data based on the method proposed in this study, as well as to evaluate the use of other drought indicators (e.g., DISS—Drought Information Satellite System [18,19]), which will help us in better understanding the response of vegetation to drought and in supporting the policy designation of water resource management and agricultural planning to reduce the impact of drought on agricultural production.

6. Conclusions

Exploring the spatiotemporal response of vegetation to flash drought is significant for water resource management, flash drought warning, and flash drought mitigation. This study proposes a method to quantify the response of vegetation to flash droughts based on the cross-spectral analysis of two time series, i.e., the ET-based drought index ESAI as the forcing and the vegetation-based drought index NAVI as the response, using remote sensing data at moderate spatial resolution (i.e., 1 km). The new method was used to explore the temporal response of vegetation to water availability during flash drought events over North China during March–September (growing season) for the period of 2001–2020. The complementarity of the time lag estimated by cross-spectral analysis and the response time index was documented. The average time lag of the response of vegetation to fluctuations in water availability during flash drought events in North China during March–September (growing season) for the period of 2001–2020, as estimated by cross-spectral analysis, was 5.9 days, which is significantly shorter than the response time estimated using the response time index method. Using the first negative NDVI anomaly to determine the response time leads to the detection of a late, irreversible stage of drought effects on vegetation, while the cross-spectral phase lag gives an earlier alert of the response to fluctuations in water availability. We also found that the time lag of the response of vegetation to water availability during flash droughts varied with vegetation types and irrigation conditions. The time lags for rainfed croplands, irrigated croplands, grass, and forest had a spatial average of 5.4, 5.8, 6.1, and 6.9 days, respectively. The findings of this study contribute to a better understanding of the mechanisms of the response of vegetation to flash droughts and support decision makers in providing early warning and timely intervention for flash droughts. While much work remains to be performed, such as using machine learning such as the CNN to investigate the response of vegetation to flash droughts, we sense that cross-spectral analysis is a generally applicable method to study forcing–response processes and a valuable addition to current methods of estimating the time lag of vegetation to flash drought. Future work will focus on exploring insights into the response of vegetation to flash droughts over broader regions as well as for different agricultural practices. Attention will also be given to developing an early warning system for flash droughts by identifying the time lag between vegetation response and water deficit based on the cross-spectral analysis.

Author Contributions: Conceptualization, P.L. and L.J.; methodology, P.L., L.J., J.L. and M.M.; validation, P.L., L.J., J.L. and M.M.; investigation, P.L., L.J., J.L., M.J. and C.Z.; data curation, P.L., L.J., M.J. and C.Z.; writing—original draft preparation, P.L.; writing—review and editing, P.L., L.J., J.L.,

M.M., M.J. and C.Z.; visualization, P.L. and L.J.; supervision, L.J., J.L., M.M., M.J. and C.Z.; project administration, L.J.; funding acquisition, L.J. All authors have read and agreed to the published version of the manuscript.

Funding: This research was jointly funded by the National Natural Science Foundation of China (NSFC) (Grant No. 42090014, 42271394), the Open Research Program of the International Research Center of Big Data for Sustainable Development Goals (Grant No. CBAS2023ORP05), the Chinese Academy of Sciences President's International Fellowship Initiative (Grant No. 2020VTA0001), and the MOST High-Level Foreign Expert Program (Grant No. G2022055010L).

Data Availability Statement: Data are available on request from the authors.

Conflicts of Interest: The authors declare no conflicts of interest.

References

1. Wilhite, D.A.; Glantz, M.H. Understanding: The drought phenomenon: The role of definitions. *Water Int.* **1985**, *10*, 111–120. [[CrossRef](#)]
2. Yuan, X.; Wang, Y.M.; Ji, P.; Wu, P.L.; Sheffield, J.; Otkin, J.A. A global transition to flash droughts under climate change. *Science* **2023**, *380*, 187–191. [[CrossRef](#)]
3. Wang, L.; Yuan, X.; Xie, Z.; Wu, P.; Li, Y. Increasing flash droughts over China during the recent global warming hiatus. *Sci. Rep.* **2016**, *6*, 30571. [[CrossRef](#)]
4. Qing, Y.M.; Wang, S.; Ancell, B.C.; Yang, Z.L. Accelerating flash droughts induced by the joint influence of soil moisture depletion and atmospheric aridity. *Nat. Commun.* **2022**, *13*, 1139. [[CrossRef](#)]
5. Yuan, X.; Wang, L.; Wu, P.; Ji, P.; Sheffield, J.; Zhang, M. Anthropogenic shift towards higher risk of flash drought over China. *Nat. Commun.* **2019**, *10*, 4661. [[CrossRef](#)]
6. Christian, J.I.; Hobbins, M.; Hoell, A.; Otkin, J.A.; Ford, T.W.; Cravens, A.E.; Powlen, K.A.; Wang, H.L.; Mishra, V. Flash drought: A state of the science review. *Wires Water* **2024**, *11*, e1714. [[CrossRef](#)]
7. Otkin, J.A.; Svoboda, M.; Hunt, E.D.; Ford, T.W.; Andersonson, M.C.; Hain, C.; Basara, J.B. FLASH DROUGHTS A Review and Assessment of the Challenges Imposed by Rapid-Onset Droughts in the United States. *Bull. Am. Meteorol. Soc.* **2018**, *99*, 911–919. [[CrossRef](#)]
8. Otkin, J.A.; Anderson, M.C.; Hain, C.; Mladenova, I.E.; Basara, J.B.; Svoboda, M. Examining Rapid Onset Drought Development Using the Thermal Infrared-Based Evaporative Stress Index. *J. Hydrometeorol.* **2013**, *14*, 1057–1074. [[CrossRef](#)]
9. Tyagi, S.; Zhang, X.; Saraswat, D.; Sahany, S.; Mishra, S.K.; Niyogi, D. Flash Drought: Review of Concept, Prediction and the Potential for Machine Learning, Deep Learning Methods. *Earths Future* **2022**, *10*, e2022EF002723. [[CrossRef](#)]
10. Otkin, J.A.; Woloszyn, M.; Wang, H.L.; Svoboda, M.; Skumanich, M.; Pulwarty, R.; Lisonbee, J.; Hoell, A.; Hobbins, M.; Haigh, T.; et al. Getting ahead of Flash Drought: From Early Warning to Early Action. *Bull. Am. Meteorol. Soc.* **2022**, *103*, E2188–E2202. [[CrossRef](#)]
11. Fu, K.Q.; Wang, K.C. Quantifying Flash Droughts Over China From 1980 to 2017. *J. Geophys. Res. Atmos.* **2022**, *127*, e2022JD037152. [[CrossRef](#)]
12. Zhang, S.Y.; Li, M.X.; Ma, Z.G.; Jian, D.N.; Lv, M.X.; Yang, Q.; Duan, Y.W.; Amin, D. The intensification of flash droughts across China from 1981 to 2021. *Clim. Dyn.* **2023**, *62*, 1233–1247. [[CrossRef](#)]
13. Zeng, Z.Q.; Wu, W.X.; Peñuelas, J.; Li, Y.M.; Jiao, W.Z.; Li, Z.L.; Ren, X.S.; Wang, K.; Ge, Q.S. Increased risk of flash droughts with raised concurrent hot and dry extremes under global warming. *Npj Clim. Atmos. Sci.* **2023**, *6*, 134. [[CrossRef](#)]
14. Christian, J.I.; Martin, E.R.; Basara, J.B.; Furtado, J.C.; Otkin, J.A.; Lowman, L.E.L.; Hunt, E.D.; Mishra, V.; Xiao, X.M. Global projections of flash drought show increased risk in a warming climate. *Commun. Earth Environ.* **2023**, *4*, 165. [[CrossRef](#)]
15. Christian, J.I.; Basara, J.B.; Hunt, E.D.; Otkin, J.A.; Xiao, X.M. Flash drought development and cascading impacts associated with the 2010 Russian heatwave. *Environ. Res Lett.* **2020**, *15*, 094078. [[CrossRef](#)]
16. He, M.Z.; Kimball, J.S.; Yi, Y.H.; Running, S.; Guan, K.Y.; Jenco, K.; Maxwell, B.; Maneta, M. Impacts of the 2017 flash drought in the US Northern plains informed by satellite-based evapotranspiration and solar-induced fluorescence. *Environ. Res. Lett.* **2019**, *14*, 74019. [[CrossRef](#)]
17. Wang, Y.M.; Yuan, X. High Temperature Accelerates Onset Speed of the 2022 Unprecedented Flash Drought Over the Yangtze River Basin. *Geophys. Res. Lett.* **2023**, *50*, e2023GL105375. [[CrossRef](#)]
18. Dabrowska-Zielinska, K.; Bochenek, Z.; Malinska, A.; Bartold, M.; Gurdak, R.; Lagiewska, M.; Paradowski, K. Drought Assessment Applying Joined Meteorological and Satellite Data. In Proceedings of the 2021 IEEE International Geoscience and Remote Sensing Symposium IGARSS, Brussels, Belgium, 11–16 July 2021; pp. 6591–6594.
19. Dabrowska-Zielinska, K.; Malinska, A.; Bochenek, Z.; Bartold, M.; Gurdak, R.; Paradowski, K.; Lagiewska, M. Drought Model DISS Based on the Fusion of Satellite and Meteorological Data under Variable Climatic Conditions. *Remote Sens.* **2020**, *12*, 2944. [[CrossRef](#)]

20. Jia, L.; Hu, G.; Zhou, J.; Menenti, M. Assessing the sensitivity of two new indicators of vegetation response to water availability for drought monitoring. In Proceedings of the Land Surface Remote Sensing, SPIE, Kyoto, Japan, 29 October–1 November 2012; pp. 85241A-1–85241A-15.
21. Kogan, F.N. Application of Vegetation Index and Brightness Temperature for Drought Detection. *Adv. Space Res.* **1995**, *15*, 91–100. [[CrossRef](#)]
22. Li, X.Y.; Li, Y.; Chen, A.P.; Gao, M.D.; Slette, I.J.; Piao, S.L. The impact of the 2009/2010 drought on vegetation growth and terrestrial carbon balance in Southwest China. *Agric. For. Meteorol.* **2019**, *269*, 239–248. [[CrossRef](#)]
23. Caccamo, G.; Chisholm, L.A.; Bradstock, R.A.; Puotinen, M.L. Assessing the sensitivity of MODIS to monitor drought in high biomass ecosystems. *Remote Sens. Environ.* **2011**, *115*, 2626–2639. [[CrossRef](#)]
24. Wu, D.; Qu, J.J.; Hao, X.J. Agricultural drought monitoring using MODIS-based drought indices over the USA Corn Belt. *Int. J. Remote Sens.* **2015**, *36*, 5403–5425. [[CrossRef](#)]
25. Mu, Q.Z.; Zhao, M.S.; Kimball, J.S.; McDowell, N.G.; Running, S.W. A Remotely Sensed Global Terrestrial Drought Severity Index. *Bull. Am. Meteorol. Soc.* **2013**, *94*, 83–98. [[CrossRef](#)]
26. Qiu, J.X.; Crow, W.T.; Wang, S.; Dong, J.Z.; Li, Y.; Garcia, M.; Shangguan, W. Microwave-based soil moisture improves estimates of vegetation response to drought in China. *Sci. Total Environ.* **2022**, *849*, 157535. [[CrossRef](#)]
27. Anderson, M.C.; Norman, J.M.; Mecikalski, J.R.; Otkin, J.A.; Kustas, W.P. A climatological study of evapotranspiration and moisture stress across the continental United States based on thermal remote sensing: 1. Model formulation. *J. Geophys. Res. Atmos.* **2007**, *112*, D10117. [[CrossRef](#)]
28. Otkin, J.A.; Anderson, M.C.; Hain, C.; Svoboda, M.; Johnson, D.; Mueller, R.; Tadesse, T.; Wardlow, B.; Brown, J. Assessing the evolution of soil moisture and vegetation conditions during the 2012 United States flash drought. *Agric. For. Meteorol.* **2016**, *218*, 230–242. [[CrossRef](#)]
29. Ji, L.; Peters, A.J. Assessing vegetation response to drought in the northern Great Plains using vegetation and drought indices. *Remote Sens. Environ.* **2003**, *87*, 85–98. [[CrossRef](#)]
30. Chen, Q.; Timmermans, J.; Wen, W.; van Bodegom, P.M. A multi-metric assessment of drought vulnerability across different vegetation types using high resolution remote sensing. *Sci. Total Environ.* **2022**, *832*, 154970. [[CrossRef](#)]
31. Vicente-Serrano, S.M.; Gouveia, C.; Camarero, J.J.; Beguería, S.; Trigo, R.; López-Moreno, J.I.; Azorín-Molina, C.; Pasho, E.; Lorenzo-Lacruz, J.; Revuelto, J.; et al. Response of vegetation to drought time-scales across global land biomes. *Proc. Natl. Acad. Sci. USA* **2013**, *110*, 52–57. [[CrossRef](#)]
32. Zhan, C.; Liang, C.; Zhao, L.; Jiang, S.Z.; Niu, K.J.; Zhang, Y.L. Drought-related cumulative and time-lag effects on vegetation dynamics across the Yellow River Basin, China. *Ecol. Indic.* **2022**, *143*, 109409. [[CrossRef](#)]
33. Zhong, S.B.; Sun, Z.H.; Di, L.P. Characteristics of vegetation response to drought in the CONUS based on long-term remote sensing and meteorological data. *Ecol. Indic.* **2021**, *127*, 107767. [[CrossRef](#)]
34. Zhao, Y.Y.; Zhu, T.J.; Zhou, Z.Q.; Cai, H.J.; Cao, Z.D. Detecting nonlinear information about drought propagation time and rate with nonlinear dynamic system and chaos theory. *J. Hydrol.* **2023**, *623*, 129810. [[CrossRef](#)]
35. Zhang, Y.; Liu, X.H.; Jiao, W.Z.; Zhao, L.J.; Zeng, X.M.; Xing, X.Y.; Zhang, L.N.; Hong, Y.X.; Lu, Q.Q. A new multi-variable integrated framework for identifying flash drought in the Loess Plateau and Qinling Mountains regions of China. *Agric. Water Manag.* **2022**, *265*, 107544. [[CrossRef](#)]
36. Zhou, Z.Q.; Shi, H.Y.; Fu, Q.; Ding, Y.B.; Li, T.X.; Liu, S.N. Investigating the Propagation From Meteorological to Hydrological Drought by Introducing the Nonlinear Dependence With Directed Information Transfer Index. *Water Resour. Res.* **2021**, *57*, e2021WR030028. [[CrossRef](#)]
37. Zhang, M.; Yuan, X. Rapid reduction in ecosystem productivity caused by flash droughts based on decade-long FLUXNET observations. *Hydrol. Earth Syst. Sc.* **2020**, *24*, 5579–5593. [[CrossRef](#)]
38. Zhang, M.; Yuan, X.; Otkin, J.A. Remote sensing of the impact of flash drought events on terrestrial carbon dynamics over China. *Carbon Balance Manag.* **2020**, *15*, 20. [[CrossRef](#)]
39. Poonia, V.; Goyal, M.K.; Jha, S.; Dubey, S. Terrestrial ecosystem response to flash droughts over India. *J. Hydrol.* **2022**, *605*, 127402. [[CrossRef](#)]
40. Sungmin, O.; Park, S.K. Flash drought drives rapid vegetation stress in arid regions in Europe. *Environ. Res. Lett.* **2023**, *18*, 014028. [[CrossRef](#)]
41. Zheng, X.D.; Huang, S.Z.; Peng, J.; Leng, G.Y.; Huang, Q.; Fang, W.; Guo, Y. Flash Droughts Identification Based on an Improved Framework and Their Contrasting Impacts on Vegetation Over the Loess Plateau, China. *Water Resour. Res.* **2022**, *58*, e2021WR031464. [[CrossRef](#)]
42. Yang, L.Y.; Wang, W.G.; Wei, J. Assessing the response of vegetation photosynthesis to flash drought events based on a new identification framework. *Agric. For. Meteorol.* **2023**, *339*, 109545. [[CrossRef](#)]
43. Zuo, D.P.; Han, Y.N.; Xu, Z.X.; Li, P.J.; Ban, C.G.; Sun, W.C.; Pang, B.; Peng, D.Z.; Kan, G.Y.; Zhang, R.; et al. Time-lag effects of climatic change and drought on vegetation dynamics in an alpine river basin of the Tibet Plateau, China. *J. Hydrol.* **2021**, *600*, 126532. [[CrossRef](#)]
44. Zhao, A.Z.; Yu, Q.Y.; Feng, L.L.; Zhang, A.B.; Pei, T. Evaluating the cumulative and time-lag effects of drought on grassland vegetation: A case study in the Chinese Loess Plateau. *J. Environ. Manag.* **2020**, *261*, 110214. [[CrossRef](#)] [[PubMed](#)]

45. Wu, D.H.; Zhao, X.; Liang, S.L.; Zhou, T.; Huang, K.C.; Tang, B.J.; Zhao, W.Q. Time-lag effects of global vegetation responses to climate change. *Glob. Chang. Biol.* **2015**, *21*, 3520–3531. [[CrossRef](#)] [[PubMed](#)]
46. Zhou, Z.Q.; Liu, S.N.; Ding, Y.B.; Fu, Q.; Wang, Y.; Cai, H.J.; Shi, H.Y. Assessing the responses of vegetation to meteorological drought and its influencing factors with partial wavelet coherence analysis. *J. Environ. Manag.* **2022**, *311*, 114879. [[CrossRef](#)]
47. van Hoek, M.; Jia, L.; Zhou, J.; Zheng, C.L.; Menenti, M. Early Drought Detection by Spectral Analysis of Satellite Time Series of Precipitation and Normalized Difference Vegetation Index (NDVI). *Remote Sens.* **2016**, *8*, 422. [[CrossRef](#)]
48. Li, H.M.; Ning, S.W.; Zhou, Y.L.; Wu, C.G.; Cui, Y.; Jin, J.L.; Xu, X.Y.; Rong, A.; Cheng, Y. Spatial and temporal analysis of drought resistance of different vegetation in the Ta-pieh Mountains based on multi-source data. *J. Water Clim. Chang.* **2023**, *14*, 4198–4219. [[CrossRef](#)]
49. Pendergrass, A.G.; Meehl, G.A.; Pulwarty, R.; Hobbins, M.; Hoell, A.; AghaKouchak, A.; Bonfils, C.J.W.; Gallant, A.J.E.; Hoerling, M.; Hoffmann, D.; et al. Flash droughts present a new challenge for subseasonal-to-seasonal prediction. *Nat. Clim. Chang.* **2020**, *10*, 191–199. [[CrossRef](#)]
50. Anderson, M.C.; Zolin, C.A.; Sentelhas, P.C.; Hain, C.R.; Semmens, K.; Yilmaz, M.T.; Gao, F.; Otkin, J.A.; Tetrault, R. The Evaporative Stress Index as an indicator of agricultural drought in Brazil: An assessment based on crop yield impacts. *Remote Sens. Environ.* **2016**, *174*, 82–99. [[CrossRef](#)]
51. Mukherjee, S.; Mishra, A.K. Global Flash Drought Analysis: Uncertainties From Indicators and Datasets. *Earths Future* **2022**, *10*, e2022EF002660. [[CrossRef](#)]
52. Joiner, J.; Yoshida, Y.; Anderson, M.; Holmes, T.; Hain, C.; Reichle, R.; Koster, R.; Middleton, E.; Zeng, F.W. Global relationships among traditional reflectance vegetation indices (NDVI and NDII), evapotranspiration (ET), and soil moisture variability on weekly timescales. *Remote Sens. Environ.* **2018**, *219*, 339–352. [[CrossRef](#)]
53. Li, P.; Jia, L.; Lu, J.; Jiang, M.; Zheng, C. A New Evapotranspiration-Based Drought Index for Flash Drought Identification and Monitoring. *Remote Sens.* **2024**, *16*, 780. [[CrossRef](#)]
54. Mu, Q.Z.; Zhao, M.S.; Running, S.W. Improvements to a MODIS global terrestrial evapotranspiration algorithm. *Remote Sens. Environ.* **2011**, *115*, 1781–1800. [[CrossRef](#)]
55. Zheng, C.L.; Jia, L.; Hu, G.C. Global land surface evapotranspiration monitoring by ETMonitor model driven by multi-source satellite earth observations. *J. Hydrol.* **2022**, *613*, 128444. [[CrossRef](#)]
56. Hu, G.C.; Jia, L. Monitoring of Evapotranspiration in a Semi-Arid Inland River Basin by Combining Microwave and Optical Remote Sensing Observations. *Remote Sens.* **2015**, *7*, 3056–3087. [[CrossRef](#)]
57. Weerasinghe, I.; Bastiaanssen, W.; Mul, M.; Jia, L.; van Griensven, A. Can we trust remote sensing evapotranspiration products over Africa? *Hydrol. Earth Syst. Sci.* **2020**, *24*, 1565–1586. [[CrossRef](#)]
58. Sriwongsitanon, N.; Suwawong, T.; Thianpopirug, S.; Williams, J.; Jia, L.; Bastiaanssen, W. Validation of seven global remotely sensed ET products across Thailand using water balance measurements and land use classifications. *J. Hydrol. Reg. Stud.* **2020**, *30*, 100709. [[CrossRef](#)]
59. Kang, S.; Eltahir, E.A.B. North China Plain threatened by deadly heatwaves due to climate change and irrigation. *Nat. Commun.* **2018**, *9*, 2894. [[CrossRef](#)] [[PubMed](#)]
60. Chen, Q.T.; Jia, L.; Menenti, M.; Hutjes, R.; Hu, G.C.; Zheng, C.L.; Wang, K. A numerical analysis of aggregation error in evapotranspiration estimates due to heterogeneity of soil moisture and leaf area index. *Agric. For. Meteorol.* **2019**, *269*, 335–350. [[CrossRef](#)]
61. Chen, Q.T.; Jia, L.; Menenti, M.; Hu, G.C.; Wang, K.; Yi, Z.W.; Zhou, J.; Peng, F.; Ma, S.X.; You, Q.A.; et al. A data-driven high spatial resolution model of biomass accumulation and crop yield: Application to a fragmented desert-oasis agroecosystem. *Ecol. Model.* **2023**, *475*, 110182. [[CrossRef](#)]
62. Bennour, A.; Jia, L.; Menenti, M.; Zheng, C.L.; Zeng, Y.L.; Barnieh, B.A.; Jiang, M. Assessing impacts of climate variability and land use/land cover change on the water balance components in the Sahel using Earth observations and hydrological modelling. *J. Hydrol. Reg. Stud.* **2023**, *47*, 101370. [[CrossRef](#)]
63. Allen, R.G.; Pereira, L.S.; Raes, D.; Smith, M. Crop Evapotranspiration-Guidelines For Computing Crop Water Requirements. *FAO Irrig. Drain.* **1998**, *56*, D05190.
64. Zhang, C.; Dong, J.W.; Ge, Q.S. Mapping 20 years of irrigated croplands in China using MODIS and statistics and existing irrigation products. *Sci. Data* **2022**, *9*, 407. [[CrossRef](#)] [[PubMed](#)]
65. Zhang, C.; Dong, J.W.; Ge, Q.S. IrriMap_CN: Annual irrigation maps across China in 2000–2019 based on satellite observations, environmental variables, and machine learning. *Remote Sens. Environ.* **2022**, *280*, 113184. [[CrossRef](#)]
66. Zhou, J.; Jia, L.; Menenti, M.; Liu, X. Optimal Estimate of Global Biome-Specific Parameter Settings to Reconstruct NDVI Time Series with the Harmonic ANalysis of Time Series (HANTS) Method. *Remote Sens.* **2021**, *13*, 4251. [[CrossRef](#)]
67. Zhou, J.; Menenti, M.; Jia, L.; Gao, B.; Zhao, F.; Cui, Y.L.; Xiong, X.Q.; Liu, X.; Li, D.C. A scalable software package for time series reconstruction of remote sensing datasets on the Google Earth Engine platform. *Int. J. Digit. Earth* **2023**, *16*, 988–1007. [[CrossRef](#)]
68. Menenti, M.; Jia, L.; Azzali, S.; Roerink, G.; Gonzalez-Loyarte, M.; Leguizamón, S.; Verhoef, W. Analysis of vegetation response to climate variability using extended time series of multispectral satellite images. *Remote Sens. Opt. Obs. Veg. Prop.* **2010**, *131*, 164.
69. Roerink, G.J.; Menenti, M.; Verhoef, W. Reconstructing cloudfree NDVI composites using Fourier analysis of time series. *Int. J. Remote Sens.* **2000**, *21*, 1911–1917. [[CrossRef](#)]

70. Menenti, M.; Azzali, S.; Verhoef, W.; Van Swol, R. Mapping agroecological zones and time lag in vegetation growth by means of Fourier analysis of time series of NDVI images. *Adv. Space Res.* **1993**, *13*, 233–237. [[CrossRef](#)]
71. Loyarte, M.M.G.; Menenti, M. Impact of rainfall anomalies on Fourier parameters of NDVI time series of northwestern Argentina. *Int. J. Remote Sens.* **2008**, *29*, 1125–1152. [[CrossRef](#)]
72. Azzali, S.; Menenti, M. Mapping isogrowth zones on continental scale using temporal Fourier analysis of AVHRR-NDVI data. *Int. J. Appl. Earth Obs. Geoinf.* **1999**, *1*, 9–20. [[CrossRef](#)]
73. Christian, J.I.; Basara, J.B.; Otkin, J.A.; Hunt, E.D.; Wakefield, R.A.; Flanagan, P.X.; Xiao, X.M. A Methodology for Flash Drought Identification: Application of Flash Drought Frequency across the United States. *J. Hydrometeorol.* **2019**, *20*, 833–846. [[CrossRef](#)]
74. Percival, D.B.; Walden, A.T. *Spectral Analysis for Physical Applications*; Cambridge University Press: Cambridge, UK, 1993.
75. White, L.B.; Boashash, B. Cross Spectral-Analysis of Nonstationary Processes. *IEEE Trans. Inform. Theory* **1990**, *36*, 830–835. [[CrossRef](#)]
76. Zhou, J.; Jia, L.; Menenti, M.; van Hoek, M.; Lu, J.; Zheng, C.L.; Wu, H.; Yuan, X.T. Characterizing vegetation response to rainfall at multiple temporal scales in the Sahel-Sudano-Guinean region using transfer function analysis. *Remote Sens. Environ.* **2021**, *252*, 112108. [[CrossRef](#)]
77. Li, S.; Zhang, L.; Huang, B.X.; He, L.; Zhao, J.F.; Guo, A.H. A comprehensive index for assessing regional dry-hot wind events in Huang-Huai-Hai Region, China. *Phys. Chem. Earth* **2020**, *116*, 102860. [[CrossRef](#)]
78. Gou, Q.; Zhu, Y.; Lü, H.; Horton, R.; Yu, X.; Zhang, H.; Wang, X.; Su, J.; Liu, E.; Ding, Z.; et al. Application of an improved spatio-temporal identification method of flash droughts. *J. Hydrol.* **2022**, *604*, 127224. [[CrossRef](#)]
79. Zhang, X.; Li, M.X.; Ma, Z.G.; Yang, Q.; Lv, M.X.; Clark, R. Assessment of an Evapotranspiration Deficit Drought Index in Relation to Impacts on Ecosystems. *Adv. Atmos. Sci.* **2019**, *36*, 1273–1287. [[CrossRef](#)]
80. Sungmin, O.; Park, S.K. Global ecosystem responses to flash droughts are modulated by background climate and vegetation conditions. *Commun. Earth Environ.* **2024**, *5*, 88. [[CrossRef](#)]
81. Yao, T.T.; Liu, S.X.; Hu, S.; Mo, X.G. Response of vegetation ecosystems to flash drought with solar-induced chlorophyll fluorescence over the Hai River Basin, China during 2001–2019. *J. Environ. Manag.* **2022**, *313*, 114947. [[CrossRef](#)] [[PubMed](#)]
82. Ho, S.; Buras, A.; Tuo, Y. Comparing Agriculture-Related Characteristics of Flash and Normal Drought Reveals Heterogeneous Crop Response. *Water Resour. Res.* **2023**, *59*, e2023WR034994. [[CrossRef](#)]
83. Kang, M.; Hao, Y.; Choi, M. The effects of flash drought on the terrestrial ecosystem in Korea. *J. Hydrol.* **2023**, *624*, 129874. [[CrossRef](#)]
84. Shi, X.L.; Ding, H.; Wu, M.Y.; Zhang, N.; Shi, M.Q.; Chen, F.; Li, Y. Effects of different types of drought on vegetation in Huang-Huai-Hai River Basin, China. *Ecol. Indic.* **2022**, *144*, 109428. [[CrossRef](#)]
85. Wu, B.F.; Ma, Z.H.; Yan, N.N. Agricultural drought mitigating indices derived from the changes in drought characteristics. *Remote Sens. Environ.* **2020**, *244*, 111813. [[CrossRef](#)]
86. Otkin, J.A.; Zhong, Y.F.; Hunt, E.D.; Basara, J.; Svoboda, M.; Anderson, M.C.; Hain, C. Assessing the Evolution of Soil Moisture and Vegetation Conditions during a Flash Drought-Flash Recovery Sequence over the South-Central United States. *J. Hydrometeorol.* **2019**, *20*, 549–562. [[CrossRef](#)]
87. Zhang, X.; Hao, Z.C.; Singh, V.P.; Zhang, Y.; Feng, S.F.; Xu, Y.; Hao, F.H. Drought propagation under global warming: Characteristics, approaches, processes, and controlling factors. *Sci. Total Environ.* **2022**, *838*, 156021. [[CrossRef](#)] [[PubMed](#)]
88. Grinsted, A.; Moore, J.C.; Jevrejeva, S. Application of the cross wavelet transform and wavelet coherence to geophysical time series. *Nonlinear Process. Geophys.* **2004**, *11*, 561–566. [[CrossRef](#)]
89. Otkin, J.A.; Zhong, Y.F.; Hunt, E.D.; Christian, J.I.; Basara, J.B.; Nguyen, H.; Wheeler, M.C.; Ford, T.W.; Hoell, A.; Svoboda, M.; et al. Development of a Flash Drought Intensity Index. *Atmosphere* **2021**, *12*, 741. [[CrossRef](#)]
90. Bartold, M.; Kluczek, M. A Machine Learning Approach for Mapping Chlorophyll Fluorescence at Inland Wetlands. *Remote Sens.* **2023**, *15*, 2392. [[CrossRef](#)]
91. Jing, X.; Zou, Q.; Yan, J.M.; Dong, Y.Y.; Li, B.Y. Remote Sensing Monitoring of Winter Wheat Stripe Rust Based on mRMR-XGBoost Algorithm. *Remote Sens.* **2022**, *14*, 756. [[CrossRef](#)]
92. Wang, Q.; Zhao, L.; Wang, M.L.; Wu, J.J.; Zhou, W.; Zhang, Q.P.; Deng, M.E. A Random Forest Model for Drought: Monitoring and Validation for Grassland Drought Based on Multi-Source Remote Sensing Data. *Remote Sens.* **2022**, *14*, 4981. [[CrossRef](#)]
93. Park, H.; Kim, K.; Lee, D.K. Prediction of Severe Drought Area Based on Random Forest: Using Satellite Image and Topography Data. *Water* **2019**, *11*, 705. [[CrossRef](#)]
94. Zhao, Y.Y.; Zhang, J.H.; Bai, Y.; Zhang, S.; Yang, S.S.; Henchiri, M.; Seka, A.M.; Nanzad, L. Drought Monitoring and Performance Evaluation Based on Machine Learning Fusion of Multi-Source Remote Sensing Drought Factors. *Remote Sens.* **2022**, *14*, 6398. [[CrossRef](#)]
95. Chen, Z.X.; Wang, G.J.; Wei, X.K.; Liu, Y.; Duan, Z.; Hu, Y.F.; Jiang, H.Y. Basin-Scale Daily Drought Prediction Using Convolutional Neural Networks in Fenhe River Basin, China. *Atmosphere* **2024**, *15*, 155. [[CrossRef](#)]

Disclaimer/Publisher’s Note: The statements, opinions and data contained in all publications are solely those of the individual author(s) and contributor(s) and not of MDPI and/or the editor(s). MDPI and/or the editor(s) disclaim responsibility for any injury to people or property resulting from any ideas, methods, instructions or products referred to in the content.